ELSEVIER

Laminar flow over a backward-facing step with a stream of hot particles

I. E. Barton
Mechanics of Fluid Research Group, Aerospace Division, Manchester School of Engineering, University of Manchester, Manchester, UK

This study predicts a variety of laminar flows that include single-phase flow with heat transfer; particle-laden flow; particle-laden flow with heat transfer, and particle-laden flow with heat transfer and associated thermal effects for a backward-facing step configuration. The thermal effects considered are buoyancy and the thermophoresis effect. The particle phase is modelled using the Eulerian–Lagrangian approach. In comparison with the single-phase flow, the introduction of low-Stokes number particles has the effect of increasing the inertia of the flow and the lower recirculation region behind the backward-facing step increases in size. Heat transfer is investigated, assuming there is a hot stream of fluid and particles entering the flow. In the present configuration, buoyancy effects suppress the various factors that cause reattachment for the main recirculation region behind the backward-facing step. The thermophoresis effect drives the particles away from the hot fluid toward colder regions, which subsequently, affects the flow field. The particles cool the fluid by effectively increasing the fluid's heat capacity.

Keywords: heat transfer; particle-laden flow; two-phase flow; backward-facing step

Introduction

Flow fields with regions of recirculation that also have heat transfer and a particulate phase are interesting relevant to combustion processes that form the foundation of combustion unit design, as well as other chemically reacting processes. The flow structure for such problems have the fundamental features of flow separation and subsequent reattachment; heat transfer and associated thermal effects, such as buoyancy; and inertial effects associated with the particulate drag. These phenomena are investigated in the present study. Additional phenomena usually associated with engineering applications, such as combustion, radiation, phase-changes and turbulence, are ignored.

Various separated flow configurations have been examined in the past. Much attention has been focused on backward-facing step flow because of its simple geometry. A common backward-facing step configuration used for numerical laminar flow studies, with an expansion ratio of 2, was initiated by the experimental and numerical study of Armaly et al. (1983) and the symposium on backward-facing steps (Morgan et al. 1984). The numerical predictions of Armaly et al. failed to give good agreement with the experimental data for intermediate- and high-Reynolds numbers, probably because of inadequate grid resolution in conjunction with the first-order upwind-differencing scheme (Leschziner 1980). Subsequent hydrodynamic predictions (Kim and Moin 1985; Orlandi 1987; Patankar et al. 1987; Durst and Pereira 1988; Guj and Stella 1988; Sohn 1988; Thangam and Knight 1989; Thangam and Knight 1990) overcame these problems, and good agreement with the experimental data was found for all but high-Reynolds numbers, probably because of three-dimensional (3-D) experimental effects.

The backward-facing step flow with an expansion ratio of 2 has become a well-established numerical benchmark, where the benchmark uses a parabola u-velocity profile set at the sudden expansion and has been used as an application test for grid adaptation techniques (Hétu and Pelletier 1992; Caruso et al. 1986; Chao and Liu 1991; Lee and Tsuei 1993). In addition, a high-Reynolds number case has been used to study the outlet boundary condition (Gartling 1990; Gresho 1991; Blosch et al. 1993; Sani and Gresho 1994).

The original problem was only hydrodynamic in nature, but it has since been developed to include the behavior of heat transfer. Initially, the buoyancy effects were ignored in the studies by Sparrow and Chuck (1987) and Kondoh et al. (1993), where the walls are treated as adiabatic except for the wall behind the backward-facing step, which is fixed to a different temperature used for the inlet flow. Vradis and VanNostrand (1993) applied a stratified temperature gradient across the inflow and studied the behaviour of the flow, assuming constant viscosity and temperature-dependent viscosity using water as the flow medium (which tends to vary more than the viscosity of air). Buoyancy-assisting effects caused by temperature variation have also become well-established numerical benchmarks for the backward-facing step geometry with an expansion ratio of two where the direction of the acceleration of gravity is parallel to the backward-facing step wall pointing away from the inlet corner. The test assumes a stratified inflow and an adiabatic backward-facing step wall and has been studied and reviewed in Leone (1990), Kobayashi et al. (1993) and Sani and Gresho (1994), amongst

Address reprint requests to Dr. Ian E. Barton, Department of Engineering, University of Cambridge, Trumpington Street, Cambridge, CB2 1PZ

Received 16 March 1996; accepted 18 November 1996

Int. J. Heat and Fluid Flow 18:400–410, 1997

655 Avenue of the Americas, New York, NY 10010

0142-727X/97/$17.00
PII S0142-727X(97)00019-2

others. This problem considers a single high-Reynolds number case with fixed parameters and was primarily developed to investigate the outlet boundary condition. A similar problem to the stratified problem has been studied by Lin et al (1990, 1991) for a low-Reynolds number flow for various directions of the acceleration of gravity. No experimental data are available for the stratified flow problem, although there are data for a similar *open* backward-facing step problem studied by Aung (1983), Hall and Pletcher (1985), and Abu-Mulaweh et al. (1993). For the open backward-facing step problem, there is a temperature differential between the inflow and the wall behind the backward-facing step, all other solid boundaries are treated as adiabatic. This configuration is similar to the experimental study of Vogel and Eaton (1985).

The concept of using an injection of fluid, for internal backward-facing step flows, which has a different temperature to the ambient conditions, was introduced by Soong and Hsueh (1993) for a similar problem with an expansion ratio of 1.5. The study also included buoyancy-assisting effects. The study uses a cold-fluid injection along the backward-facing step wall in order to control heat transfer and the recirculation region.

Finally, the backward-facing step geometry with an expansion ratio of two has been used in an experimental study by Ruck and Makiola (1988). For very dilute gas–solid turbulent flows, the loading of the particles is very small, and the behaviour of the particles is assumed to have a negligible effect on the flow. Unfortunately, this seems to be the only particle-laden study available for this particular backward-facing step flow configuration.

There are many examples of predictions (usually with limited experimental data) of solid–gas flows especially for engineering applications. Unfortunately, this is not the case for laminar or technical studies of the backward-facing step configuration of Armaly et al. (1983). Usually, the loading of the particles in a solid–gas flow study is high enough to affect the behavior of the flow, this can be successfully modeled using the Eulerian–Lagrangian approach, which is also referred to as discrete particle model or Particle-Source In Cell (PSIC) method, which is described in Crowe et al. (1977) and is discussed later. The method has been applied to a range of applications from simple hydrodynamic problems discussed in Durst et al. (1984) and Celik (1988), to cyclone units (Boysan et al 1982), to small combustion units (Abbas et al. 1980; Lockwood et al. 1980, Gosman and Ioannides 1983), to full-scale furnaces (Boyd and Kent 1986).

The present study predicts a variety of different types of laminar flow over a backward-facing step. The investigation considers flows that have the addition of particles. The initial temperature of the particles may be set to a different temperature than the inlet fluid temperature, in which case, heat transfer is predicted. Thermodynamic forces, such as buoyancy, are also modelled.

Analysis

Figure 1 shows schematically the flow configuration considered in the present study, which is a two-dimensional (2-D) backward-facing step geometry with an expansion ratio of two. The origin of the Cartesian coordinate system used in the present study lies at the base of the step. The inlet channel is $3h$ in length and the outlet channel is $32h$ in length, where h is the step-height. The inlet channel was used to prevent effects downstream of the sudden expansion propagating upstream. The flow entering the channel is assumed to be fully-developed and is described using u-velocity parabola. The flow is steady; laminar and physical constants, such as density and viscosity, are assumed

Notation

c_p^f, c_p^p	specific heat capacity of the fluid and particle
c^*	ratio of particle to specific heat capacity of fluid
d_p	particle diameter
E	expansion channel number
g	acceleration of gravity
h	step-height length
K	thermophoresis constant
k	thermal conductivity
m_p	particle mass
Nu	Nusselt number
$\dot{n}_s$	number flux along a particle trajectory
Pe	Peclet number
Pr	Prandtl number
p	pressure
q	profile parameter
Re	Reynolds number
Ri	Richardson number
S_p	particle source term
Stk	Stokes number
T	temperature
t	time
u	velocity
V	void fraction
x	x-coordinate position
x_1, x_2, x_3	lower reattachment, upper separation, and upper reattachment lengths
y	y-coordinate position

Greek

β	volumetric expansion coefficient
Δt	time-step interval
ΔT_{inlet}	maximum temperature difference at the inlet
μ	dynamic viscosity
ν	kinematic viscosity
ρ	fluid density
τ_p	particle relaxation time
ϕ	quantity relating to temperature difference or particle concentration

Subscripts

f	fluid
inlet	inlet condition
max	maximum
o	average flow conditions
p	particle

Superscripts

f	fluid
n	time-level , (nth level)
*	nondimensionalised term or predicted term

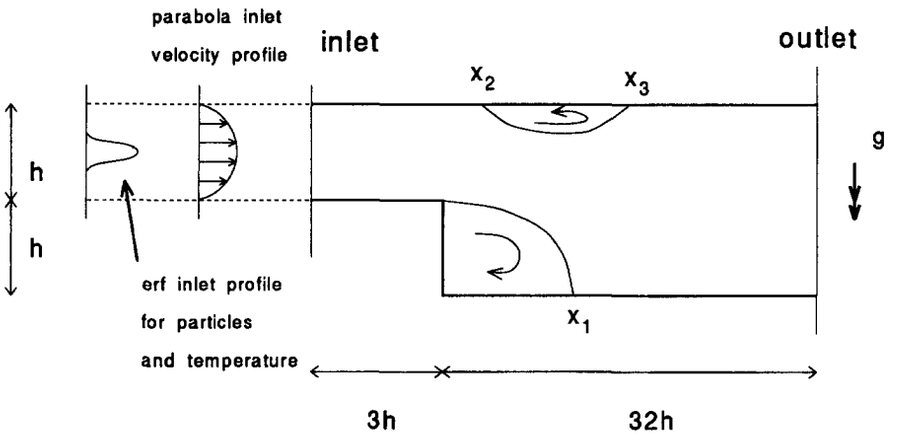

Figure 1 Schematic of the flow configuration illustrating the particle stream and recirculation regions

to remain fixed for a particular flow prediction. The buoyancy effect is, therefore, modelled using the Boussinesq approximation to account for the density variation in the flow. The step walls and solid boundaries are treated as adiabatic. The flow has a main reattachment point downstream of the backward-facing step, and for higher-Reynolds numbers where the adverse pressure gradient is strong enough, there is also an upper recirculation region. These recirculation regions are illustrated in the schematic.

The differential governing equations for the fluid phase are the equations of continuity; the Newtonian-momentum equations, and the governing equation for the temperature, which can be expressed in nondimensional vectorial notation as follows:

$$\nabla \cdot \mathbf{u} = 0 \tag{1}$$

$$\mathbf{u} \cdot \nabla \mathbf{u} = -\nabla p + \mathrm{Re}^{-1} \nabla^2 \mathbf{u} + \mathrm{Ri}\mathbf{k}T + S_p^u (h/\rho u_o^2) \tag{2}$$

$$\mathbf{u} \cdot \nabla T^* = \mathrm{Pe}^{-1} \nabla^2 T^* + S_p^T (h/c_p^f \rho u_o \nabla T_{\mathrm{inlet}}) \tag{3}$$

where $\mathbf{k}$ is the unit vector in the y-direction, $\mathrm{Re} = u_o h/\nu$ is the Reynolds number, $\mathrm{Ri} = \beta g \Delta T_{\mathrm{inlet}} h/u_o^2$ is the Richardson number, and $\mathrm{Pe} \equiv \mathrm{Pr}\,\mathrm{Re}$ is the Peclet number, where Pr is the Prandtl number. The velocity terms are nondimensionalized using u_o, and the temperature terms using $\Delta T_{\mathrm{inlet}}$. The physical properties are u_o the average inlet velocity, h the step height, ν fluid viscosity, β volumetric expansion coefficient, g acceleration of gravity, $\Delta T_{\mathrm{inlet}}$ the maximum temperature difference at the inlet, ρ the density of the fluid, and c_p^f the specific heat capacity of the fluid.

The presence of the particles have been introduced via source terms, S_p^u and S_p^T, which describe the particle–drag interaction and the particle–fluid heat exchange respectively. The volume of the particles have been neglected in the governing equations.

The stream profile for the temperature of the particles and fluid as well as the particles number density is modelled using an erf function:

$$\phi = \phi_{\max} \exp\left(-q \left(\frac{\Delta y}{h} \right)^2 \right) \tag{4}$$

where Δy is the distance away from the middle of the inlet channel, and the ϕ quantity is the inlet temperature difference or particle void fraction. Values below $0.05\phi_{\max}$ are truncated to zero. The q parameter was set to produce a slightly diffuse stream profile. The void fraction V is the volume displaced by the particles-per-unit volume and is generally used to describe the quantity of particles instead of the particle number density, refer to Durst et al. (1984).

Numerical method

The gas–solid flow is solved using the Eulerian–Lagrangian approach, which solves the fluid phase using an Eulerian solution procedure and introduces the presence of the particles by means of additional source terms. The presence of the particles is modelled using the Lagragian methodology, where individual particle trajectories are calculated. After the velocities and trajectories have been calculated, the extra source terms for the flow field can then be solved. Thus, the numerical method has two distinct parts. The solution algorithm for the fluid phase is initially considered.

The fluid phase

The solution method of the governing equations is the SIMPLE (Semi-Implicit Method for Pressure Linked Equations) algorithm. The SIMPLE method is based on a parabolic procedure developed by Patankar and Spalding (1972). The SIMPLE algorithm and other numerical details commonly used in conjunction with the algorithm are described in some detail in Patankar (1980), and only a brief account of the method and numerical details used in the present study is given here.

The governing partial differential equations are integrated over control volumes that form a computational grid over the problem domain. The grid used in the present study is shown in Figure 2; the figure shows every other grid line. The control volumes are clustered in greater number close to the solid boundaries where the velocity gradients are at their greatest. The present study used 100×80 grid points for the present computations. The grid dependency of computations were tested using a similarly clustered grid using 40×40 and 80×60 grid points, a similar grid dependency study has been carried out in Barton (1996a). The 80×60 grid results predicted similar reattachment and separation lengths compared with the 100×80 grid, the differences are typically less than 1%. The largest differences tend to occur for the separation length x_2, for some of the higher Reynolds numbers, the differences between the two sets of results are of the order 2%. The differences in the results are sufficiently small for the 100×80 grid to give reliable results. Comparisons were undertaken for all simulations; introduction of a particulate phase and heat transfer did not increase greatly the discrepancy. In the case of heat transfer, this is not surpris-

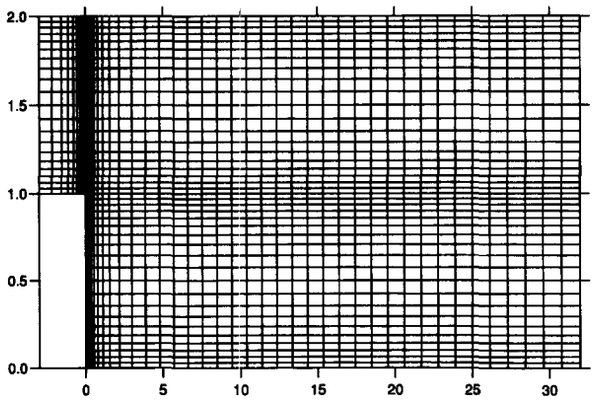

Figure 2 Computational grid using a grid density of 1 : 2

ing, because the Prandtl number is set to 0.7; therefore, the diffusive forces in the temperature conservation equation are larger than those experienced by the momentum equations.

The velocity and pressure terms are located on a staggered grid system developed by Harlow and Welch (1965). The solution procedure requires interpolation between various points that is achieved by second-order upwind differencing (Shyy 1985) for the convective terms; second-order accurate central-differencing is used for the diffusive terms. Although the grid used in the present investigation is only approximately twice as fine as the grid used in the study by Armaly et al. (1983) because a second-order upwind differencing scheme is used, the local truncation error is at least two orders of magnitude smaller. The discretized equations are solved in an iterative procedure that starts with the solution of the velocities using the current pressure field. Next, using a pressure correction equation derived from the continuity equation, the pressure and velocities are corrected so that they satisfy continuity. The whole procedure is repeated until the pressure and velocity fields converge to a final solution.

The inlet velocity terms use a prescribed u-velocity profile. No-slip boundary conditions are applied at the solid boundaries. The outlet channel is $32h$ long; this seems to be sufficiently long to prevent errors caused at the outlet condition propagating upstream.

The outflow boundary condition developed and discussed in Barton (1995) was applied. In short, the extrapolated velocities at the outlet are calculated using the following fit.

$$u = A + \frac{B}{(x/\Delta x)} + \frac{C}{(x/\Delta x)^2} \tag{5}$$

In the extrapolation, the four velocity positions upstream of the outflow boundary are used. The velocity position the farthest from the outflow boundary is used as the datum position for x, the velocity values at the other three positions are used for extrapolation calculation. The Δx term is the cell length adjacent to the outflow boundary. Therefore, if uniform cells are used near the exit region, the extrapolated velocity value is estimated by (using compass notation),

$$u_{\text{exit}} = \frac{27u_W - 12u_{WW} + u_{WW}}{16} \tag{6}$$

and is then corrected to ensure that overall flux is conserved. This formation seems to reduce numerical errors near the outflow boundary (Barton 1995).

The temperature field

The governing differential equation for the temperature of the fluid is coupled with the momentum equations through buoyancy. The acceleration of gravity is taken to be parallel to the step wall away from the inlet similar to other studies (Leone 1990; Kobayashi et al. 1993; Sani and Gresho 1994). The SIMPLE algorithm incorporates the solution of the temperature field at the end of each cycle, which allows the temperature and velocity fields to become gradually coupled. The buoyancy effect is introduced using the Boussinesq approximation $\rho_o g\beta(T - T_o)$ where β is set as $1/T$ (from the ideal gas law). The present study investigates constant $(\rho_o g/T_o)$ values at various Reynolds numbers and also a constant Richardson number of 9/16, which is the same value used in the numerical benchmark tests by Leone, Kobayashi et al., and Sani and Gresho. Adiabatic boundary conditions are applied at the solid boundaries.

The sets of algebraic equations formed from the momentum and temperature conservation equations are solved by sweeping through the computational domain with repeated application of a tridiagonal matrix algorithm, referred to as the Thomas algorithm, described in Anderson et al. (1984). The convergence is assumed when the average field residuals for the fluid properties (u, v, p, T) reduce to 1×10^{-5} of their initial value.

The particle phase

In the Eulerian–Lagrangian approach, the particles are solved in a Lagrangian frame. The method was proposed by Migdal and Agosta (1967) and was developed into the PSIC method. The technique is described in detail elsewhere (Crowe et al. 1977); only a brief summary is given here. The present study follows the details described in Durst et al. (1984). The particle phase is solved using the equation of motion for a single particle. For a particle heavier than the surrounding fluid, which is small in diameter, this can be described using Stokes Law, provided the particle Reynolds number is less than unity:

$$m_p \frac{\mathrm{d}u_p}{\mathrm{d}t} = 3\pi\mu d_p(u_f - u_p) \tag{7}$$

The particle Reynolds number is defined using the particle's diameter as a length scale and the velocity slip between the phases as the velocity term (Soo 1982). The particle's mass, velocity, and diameter are m_p, u_p, and d_p, respectively. Assuming an initial velocity and position at the inlet boundary the equation of motion can then be integrated to find the velocity and position of the particle through the domain.

The equation of motion is integrated using a new predictor–corrector exponential Lagrangian tracking scheme presented in Barton (1996b); the scheme is summarized in the appendix. The new integration scheme reduces the numerical error by one or two orders of magnitude and has been successfully implemented in Barton (1996a).

Repeating the integration procedure for a number of starting positions, the source terms can be calculated successfully. The principle underlying the source terms is that a single particle trajectory represents a "parcel of particles," its magnitude, therefore, depends upon the inlet concentration of particles. The particle momentum source terms are derived from the transfer of momentum through viscous action. A control volume, therefore, has an extra source term described by the time integral:

$$S_p = -3\pi\mu\, \mathrm{d}_p \dot{n}_s \int_{t_{\text{in}}}^{t_{\text{out}}} (u_f - u_p)\, \mathrm{d}t \tag{8}$$

where the t_{in} and t_{out} times are when the particle enters and leaves the control volume. The $\dot{n}_s$ term is the number of particles travelling along a trajectory per second, which incorporates the "parcel of particles" concept (Durst et al. 1984). The source terms are incorporated into the single-phase solution procedure after the temperature field has been calculated.

The particle's temperature is assumed to be governed by:

$$m_p c_p^p \frac{dT_p}{dt} = \mathrm{Nu}\, \pi k\, d_p (T_f - T_p) \tag{9}$$

where Nu is the Nusselt number of particle and is set to 2 (Soo 1982), k is the thermal conductivity of the fluid, and c_p^p is the specific heat capacity of the particle. The equation is in the same form as the equation of motion, and it can be integrated in a similar way. The additional source term for the temperature governing equation is also in a similar form as Equation 8:

$$S_p^T = -3\pi\mu\, d_p \dot{n}_s \left(\frac{\mathrm{Nu}}{3\,\mathrm{Pr}}\right) c_p^f \int_{t_{in}}^{t_{out}} (T_f - T_p)\, dt \tag{10}$$

where Pr is the fluid's Prandtl number. An additional nondimensional term, c^*, which is the ratio of the particle's specific heat capacity to that of the fluid, is also required because of the introduction of the Prandtl number.

The numerical time-step Δt was set so that the particle takes approximately ten time-steps to cross a control volume. The initial starting location of the particle is set on the inlet boundary and the velocity of the particle is set to the same as the fluid. Also, the initial temperature of the particle is set to the same as the surrounding fluid. The particle phase uses 20 starting locations per control volume that are evenly spaced in an individual control volume, a total of 260 trajectories are solved.

Parameters

- channel lengths, $L_1 = 3$, $L_2 = 32$
- expansion ratio, $E = 2$
- inlet Reynolds number, Re = 50, 100, 200, 300, 400, 500, 600, 700
- Stokes number, Stk = 1×10^{-4}, 1×10^{-3}
- void fraction maximum, $V_{max} = 50 \times 10^{-3}$, 5×10^{-3}
- profile parameter, $q = 50$, 100
- Nusselt number, Nu = 2
- Prandtl number, Pr = 0.7
- specific heat capacity ratio, $c^* = 4$
- Richardson number[1], Ri = $8 \times 10^4/\mathrm{Re}^2$
- Richardson number[2], Ri = 9/16 (constant)
- thermophoresis constant, $K = 1.0$

The Richardson number was studied for constant physical properties; e.g., constant temperature differential, gravity constant etc., which would probably be used in an experimental study, using constant properties results in a varying Richardson number[1]. In addition, the Richardson number was fixed, Ri = 9/16, which is the same value used in the benchmark studies of Leone (1990), Kobayashi et al. (1993) and Sani and Gresho (1994). The thermophoresis constant is discussed later.

Results

Hydrodynamic single-phase flow: case (1)

The laminar single-phase flow problem has been studied extensively. The behaviour of the flow has been discussed in detail elsewhere (Armaly et al. 1983; Thangam and Knight 1989, 1990) (see Sohn 1988 for a presentation of pressure contours). The behaviour of the flow, therefore, is only briefly summarized. The flow behaves similar to an open backward-facing step flow for low-Reynolds numbers. The flow separates at the corner of the step and reattaches further downstream, as shown in Figure 3 for Re = 300 (the streamlines in the vortex are at intervals ten times smaller than the streamlines in the free stream). The reattachment length increases almost linearly with Reynolds number. The slight nonlinear trend is caused by viscous drag along the upper wall boundary, which forces flow away from the upper wall. The downwards movement inhibits the growth of the lower reattachment length and has been studied in Thangam and Knight (1989). For higher-Reynolds numbers, the adverse pressure gradient caused by the sudden change in geometry is strong enough to cause the flow to separate from the upper wall boundary. The flow reattaches farther downstream and forms an upper recirculation region. The centre of the recirculation region moves downstream with increasing Reynolds number (because the adverse pressure gradient increases), and its size increases. The upper recirculation inhibits the growth lower recirculation region, and the lower reattachment length deviates further from the open case (Thangam and Knight 1989; Barton 1994).

The reattachment and separation positions are summarized in Figure 4 with the experimental data of Armaly et al. (1983) and the numerical results of Guj and Stella (1988) for a numerical comparison. For low-Reynolds numbers, the various results are in good agreement, but the results tend to deviate for higher-Reynolds numbers; in comparison with the experimental data, the numerical predictions tend to deviate for Reynolds numbers above Re = 500. This is probably caused by three-dimensional (3-D) experimental effects. The present predictions use an inlet channel $3h$ long, which probably causes a slight difference in the numerical results. Guj and Stella set the inlet boundary condition at the step; this prevents downward movement of flow at the step, which tends to suppress the growth of the upper recirculation region. There are other possibilities for the differences, such as the differencing scheme, grid distributions, and even a slight difference in the expansion ratio.

Transport of hot fluid: case (2)

The transport of hot fluid is considered for no thermal effects, e.g., Ri = 0. The behaviour of the flow is, therefore, the same as case (1). The temperature contours for Re = 300 are shown in

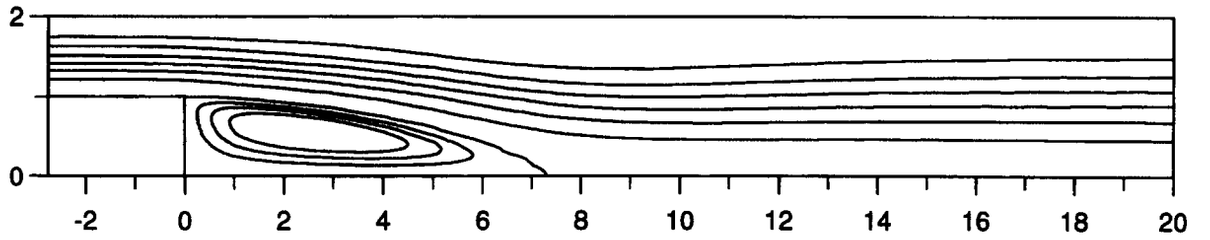

Figure 3 Streamlines for the isothermal single-phase flow, Re=300

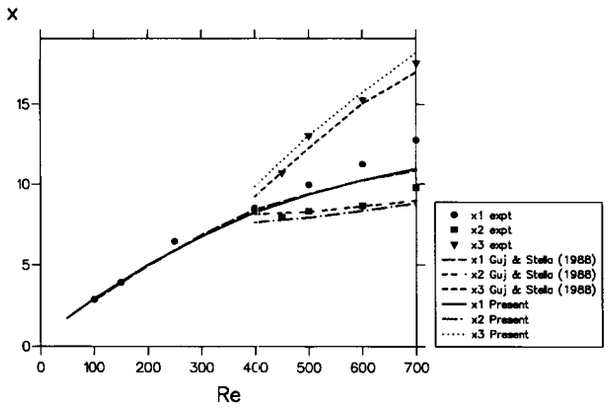

Figure 4 Isothermal single-phase flow reattachment and separation lengths for various Reynolds numbers

Figure 5. The figure shows how the hot fluid diffuses in the inlet channel forming an almost symmetrical profile, and the boundary-layer growth further downstream prevents hot flow close to the lower boundary. The hot fluid is pulled towards the upper boundary, partly because the flow moves upward downstream of the lower reattachment or because of the upper reattachment if it forms. The flow becomes fairly stratified further downstream of the recirculation regions.

Isothermal particle-laden flows

The effect of introducing the particles into the flow is considered for the following test cases: (3) Srk $= 1 \times 10^{-4}$, $V_{max} = 50 \times 10^{-3}$, $q = 100$; (4) Stk $= 1 \times 10^{-3}$, $V_{max} = 50 \times 10^{-3}$, $q = 100$; and (5) Stk $= 1 \times 10^{-4}$, $V_{max} = 5 \times 10^{-3}$, $q = 50$. The numerical tests (3) and (4) use a very fine but dense cloud of particles. This formation is similar to a particle formation referred to as a "particle rope." The void fraction is sufficiently high for the likelihood of interparticle collisions to occur; however, this and Brownian motion have been ignored. The interparticle collisions interaction has been considered by Mostafa (1991) for turbulent diffuse clouds, because the cloud of particles is neither diffuse nor turbulent, the assumption that the interparticle collisions can be ignored has a slightly greater validity.

Case (3) and (4)

The results for cases (3) and (4) are virtually identical. The separation and reattachment lengths are summarized in Tables 1 and 2. The largest difference in reattachment and separation length is about 0.1%, the difference is usually about 0.01–0.05%, and the largest differences tend to occur for the upper separation length x_2. The reason the results are virtually the same is because the coefficient of the source term in Equation 8 is inversely proportional to the Stokes number. It is clear from examining the equation of motion that low-Stokes number particles tend to follow the flow; therefore, $du_p/dt \approx du_f/dt$. This implies the velocity slip will be approximately proportional to the Stokes number for low-Stokes number particles moving freely in a flow field. The source term's coefficient and integral combined, therefore, imply the particle source term remains constant for low-Stokes numbers, provided no other significant forces are present.

Introduction of the particles encourages growth of the lower recirculation region, because the particles effectively increase the inertia of the flow over the lower recirculation region. The increase in inertia is caused by the particles passing the sudden expansion region and "overshooting" the streamlines. This creates a downstream drag force on the flow. The flow is, therefore, faster over the lower recirculation region, generating a stronger and longer lower recirculation region of about $0.7h$ in comparison with the single-phase case for Re = 300 and above, below Re = 300 the perturbation decreases fairly linearly. The downstream drag force is also present farther downstream, and as the particles flow past the upper recirculation region, this generates a stronger upper recirculation region, which tends to move downstream with increasing Reynolds number. The upper separation position x_2 is strongly influenced by the lower reattachment, which prevents the upper recirculation position region moving considerably upstream.

Table 1 Reattachment and separation lengths for various Reynolds numbers, case (3)

Re	x_1	x_2	x_3
50	1.915	—	—
100	3.257	—	—
200	5.531	—	—
300	7.414	—	—
400	8.913	7.836	11.662
500	10.045	8.190	14.976
600	10.894	8.642	17.847
700	11.624	9.127	20.418

Table 2 Reattachment and separation lengths for various Reynolds numbers, case (4)

Re	x_1	x_2	x_3
50	1.917	—	—
100	3.256	—	—
200	5.530	—	—
300	7.413	—	—
400	8.911	7.833	11.665
500	10.034	8.177	14.984
600	10.889	8.640	17.848
700	11.618	9.121	20.419

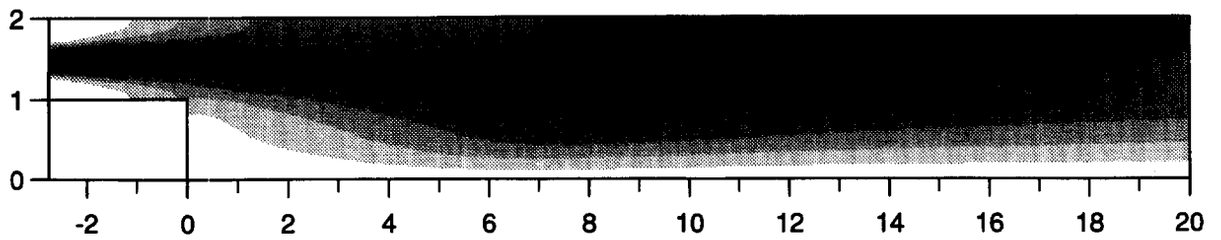

Figure 5 Temperature contours for Re=300, case (2)

Case (5)

A wider stream of particles with a lower void peak value of 5×10^{-3} was investigated for test case (5). The lower void fraction in comparison with the previous test cases means the flow field is less perturbed from the single-phase flow. Otherwise, case (5) behaves in a manner similar to cases (3) and (4). The reattachment and separation lengths are summarized in Table 3. The lower reattachment seems to be linearly perturbed from the single-phase case for Reynolds numbers of Re = 300 and below, above Re = 300, the lower reattachment length is $0.1h$ longer than the single-phase case (several times smaller than the previous two cases). The upper recirculation region grows in size approximately $0.3h$, remaining constant for all Reynolds numbers. Growth in the upper recirculation region occurs mainly in the upper reattachment length x_3. The separation length x_2 moves slightly upstream with respect to the lower length x_1, but essentially, the separation length seems to depend mainly upon the position of lower reattachment. The particle-laden flow is perturbed only slightly from the single-phase flow, and the presence of the particles does not significantly alter the streamlines or pressure contours. The pressure contours for Re = 500 are shown in Figure 6, which are virtually the same as the single-phase case.

Heat transfer and particle laden flows

The effects of buoyancy and thermophoresis are now considered in test cases (6)–(9). Parameters used for the various case studies are: (6) $\mathrm{Stk} = 1 \times 10^{-4}$, $V_{\max} = 5 \times 10^{-3}$, $q = 50$, no buoyancy effects ($\mathrm{Ri} = 0$); (7) $\mathrm{Stk} = 1 \times 10^{-4}$, $V_{\max} = 5 \times 10^{-3}$, $q = 50$, buoyancy ($\mathrm{Ri} = 8 \times 10^5/\mathrm{Re}^2$); (8) $\mathrm{Stk} = 1 \times 10^{-4}$, $V_{\max} = 5 \times 10^{-3}$, $q = 50$, buoyancy ($\mathrm{Ri} = 8 \times 10^5/\mathrm{Re}^2$), thermophoresis; and (9) $\mathrm{Stk} = 1 \times 10^{-4}$, $V_{\max} = 5 \times 10^{-3}$, $q = 50$, buoyancy ($\mathrm{Ri} = 9/16$). The temperature field predicted in test case (6) is not coupled with the flow field; therefore, the uncoupled transport effects of the temperature field can be used as comparison. Test cases (7) and (8) assume constant physical properties, such as a length scale, and the acceleration of gravity, consequently, the Richardson number varies with the inverse of Re^2. Case (9) uses a constant Richardson number of $\mathrm{Ri} = 9/16$, which is the same value used in the benchmark studied by Leone (1990), Kobayashi et al. (1993) and Sani and Gresho (1994).

Table 3 Reattachment and separation lengths for various Reynolds numbers, case (5)

Re	x_1	x_2	x_3
50	1.745	—	—
100	2.961	—	—
200	5.074	—	—
300	6.861	—	—
400	8.328	7.560	10.154
500	9.229	7.867	13.360
600	10.294	8.294	16.045
700	11.034	8.761	18.460

Case (6)

The flow field is not coupled to the temperature field, and the description of the hydrodynamic nature of the flow given in case (5) is applicable to case (6). The hot fluid and particles are transported downstream from the inlet. The hot temperature field is dependent upon subsequent convection and diffusion processes; whereas, the motion of the particles is dependent upon the convection transport only. The diffusion process tends to dominate the temperature field, and the sharp hot fluid profile at the inlet rapidly diffuses. The ratio of inertia-to-diffusion experienced by the temperature field is described by the Peclet number, $\mathrm{Pe} \equiv \mathrm{Pr}\,\mathrm{Re}$, because the Prandtl number is constant, the Peclet number is, therefore, dependent upon the Reynolds number. This is reflected in the temperature field results, a low-Reynolds number result only transports the effects of the hot fluid no farther than upstream of the sudden expansion; whereas, a high-Reynolds number result can transport fairly significant temperature effects almost to the domain's exit.

Case (7)

The buoyancy effects generate upward movement of flow upstream near the sudden expansion. Upward movement of flow delays the reattachment downstream of the sudden expansion, although the upward force is not evident in the particle's pathlines. The concentration contours of the particles are shown in Figure 7 for Re = 500. Because the Richardson number is proportional to the inverse of Re^2, the strength of the buoyancy effects decreases with Reynolds number. The low-Reynolds number results, therefore, have lower reattachment lengths significantly downstream of the isothermal particle-laden flow and single-phase flow. The reattachment and separation lengths are summarized in Table 4. The larger lower recirculation region for the intermediate Reynolds numbers suppresses the upper recirculation region, and the upper recirculation region forms for Reynolds numbers of Re = 600 and above. This is caused by the significant suppression of the adverse pressure gradient, which is shown in Figure 8 for Re = 500. The Re = 700 results are similar to the hydrodynamic particle-laden flows. Separation of the upper recirculation region seems to be strongly influenced by the lower reattachment position, because a displacement in the position of the lower reattachment length is similar to displacement in the position of the upper separation point.

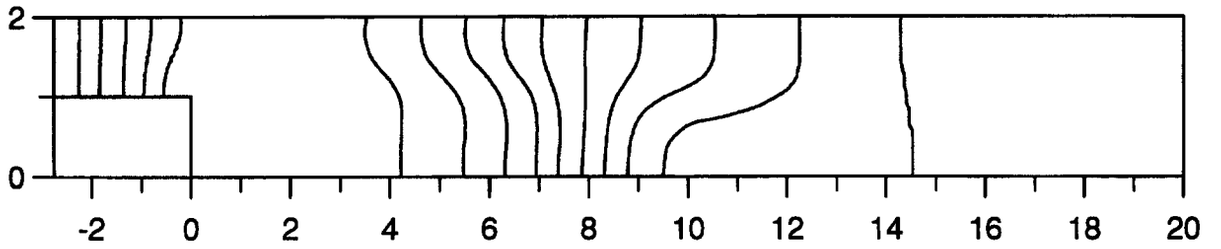

Figure 6 Pressure contours for Re=500, case (5)

Table 4 Reattachment and separation lengths for various Reynolds numbers, case (7)

Re	x_1	x_2	x_3
100	9.220	—	—
200	7.368	—	—
300	8.947	—	—
400	10.145	—	—
500	11.178	—	—
600	11.763	9.969	15.361
700	11.338	9.017	17.665

Case (8)

The previous test case study is repeated with introduction of the thermophoresis effect described in Soo (1982). The thermophoresis effect is a force exerted on the particle caused by variation of the surrounding fluid temperature. The effect is estimated to be four orders of magnitude stronger than the Brownian motion effect, which has been ignored. Ideally, the thermophoresis effect should be treated in the Eulerian frame, because it is a diffusion-type force. The particles, however, are solved in the Lagrangian frame, so the effect is added as a velocity perturbation to the solution of the current particle's velocity. Where the velocity perturbation is given by:

$$\Delta u_i = -\frac{K}{T}\nu\frac{\partial T}{\partial x_i} \tag{11}$$

where K is the thermophoresis constant, which is set at 1.0 (Walker et al. 1980). The velocity perturbation is negatively dependent upon the surrounding fluid temperature gradient and is equivalent to the Brownian motion effect, which is dependent upon the particle concentration gradient. The force has the effect of diffusing the particles away from hot fluid towards cold fluid. In comparison with the previous test case, the thermophoresis effect has only a significant effect on the particles in the main channel. It was anticipated that the particles would disperse in the inlet channel because of the strong temperature gradients in the y-direction. There was some evidence that this occurred, although the effect is not significant, because no strong temperature gradients in the y-direction actually occur across the stream of particles. This is because the sharp temperature profile rapidly diffuses outwards; whereas, the particles tend not to diffuse outwards. Thus, the temperature variation remains fairly constant in the y-direction across the particles. The hot fluid's temperature decreases downstream from the inlet, and the outlet temperature is virtually the same as ambient conditions. The gradual decrease in temperature for the hot stream of fluid causes a small thermophoresis effect on the particles. The particles gain momentum in the x-direction, and this results in a higher inertia of flow and, consequently, a longer reattachment length of about $0.5h$ to $1.5h$ in comparison with test case (7). The largest differences occur for the low-Reynolds numbers. The reattachment and separation lengths are summarized in Table 5. The faster stream of particles do not seem to have a significant effect on the upper recirculation region, however, because the thermophoresis effect is insignificant when the particles pass the upper recirculation region. The upper recirculation region simply moves downstream in response to the longer lower recirculation length. The temperature of various particles with respect to their x-coordinate is shown in Figure 9. The figure shows 1 in 20 temperature histories. Initially, the hottest particle is in the middle of the stream, but it rapidly cools, because the peak fluid temperature rapidly diffuses outwards. The surrounding particles have a significant effect on the temperature of the fluid, because, as the hot fluid diffuses outwards, it passes cooler particles, which effectively cools the flow despite the fact that the particles are actually hotter than ambient conditions. The flow where the particles are present farther downstream now behaves as if its heat capacity has increased; any energy that heat up the flow must also heat up the particles.

Case (9)

In contrast with the previous two test cases, the Richardson number is set to a constant value of $\mathrm{Ri} = 9/16$. The results for case (9), therefore, predict a similar lower reattachment length of $8.2h$ for $\mathrm{Re} = 400$ in comparison with case (7), because the Richardson numbers for both cases are of the order 0.5. The reattachment and separation lengths are summarized in Table 6. For higher-Reynolds numbers, case (9) predicts longer, lower reattachment lengths, and the first predicted upper recirculation region is for $\mathrm{Re} = 700$; whereas, for lower-Reynolds numbers, case (9) predicts shorter lower reattachment lengths.

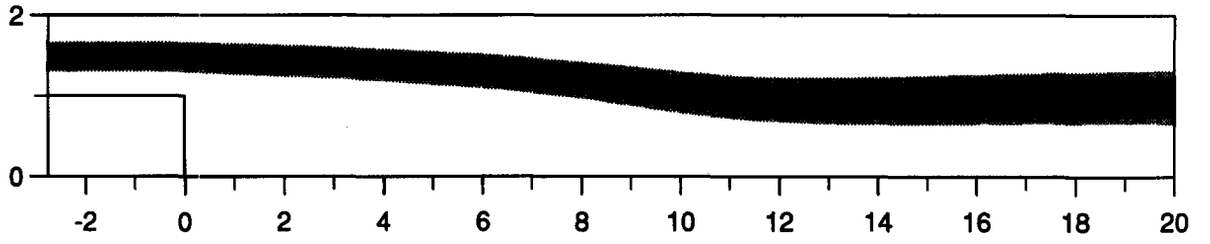

Figure 7 Particle concentration contours for Re=500, case (7)

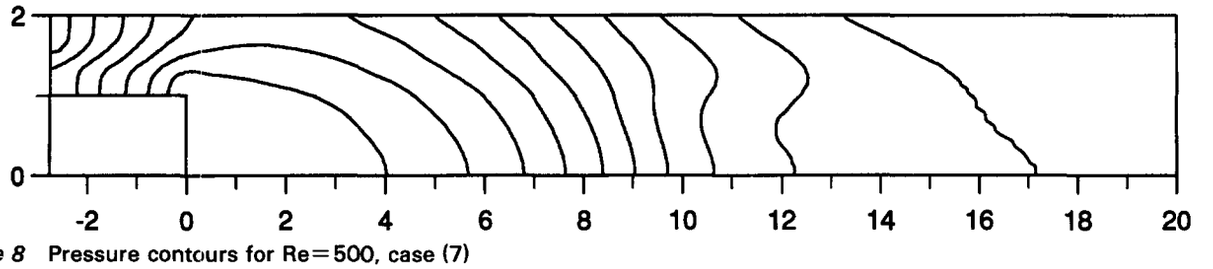

Figure 8 Pressure contours for Re=500, case (7)

Table 5 Reattachment and separation lengths for various Reynolds numbers, case (8)

Re	x_1	x_2	x_3
100	10.867	—	—
200	8.296	—	—
300	9.683	—	—
400	10.838	—	—
500	11.759	—	—
600	12.291	10.542	16.094
700	12.125	9.820	18.392

Table 6 Reattachment and separation lengths for various Reynolds numbers, case (9)

Re	x_1	x_2	x_3
50	1.733	—	—
100	3.043	—	—
200	5.431	—	—
300	8.218	—	—
400	10.210	—	—
500	12.589	—	—
600	14.594	—	—
700	13.608	11.163	15.437

Although the Richardson number is constant, the buoyancy effect is not. The lower-Reynolds number results are only slightly perturbed from the equivalent single-phase and particle-laden flows. The low-Reynolds number cases have such a low inertia that the hot fluid can diffuse almost completely in the inlet channel; and therefore, there is no temperature differential at the sudden expansion or over the lower recirculation region to cause an upward buoyancy force. As the Reynolds number increases, the hot fluid is successfully transported downstream, and the buoyancy force significantly affects the lower reattachment length. In comparison with the isothermal, particle-laden flow, differences increase superlinearly with Reynolds number, suddenly dropping when the upper recirculation region forms. The buoyancy force essentially has the effect of suppressing the downward motion of flow caused by viscous drag from the upper solid boundary. Consequently, the present results have a stronger linearity with Reynolds number, even for Reynolds numbers of Re = 300 and below. For Re = 400 and above, the equivalent single-phase and particle-laden results predict the formation of an upper recirculation region, which further inhibits the linear growth of the lower reattachment length. The buoyancy force, however, suppresses this formation, and again, the lower reattachment length is allowed to grow with greater linearity.

The temperature contours for Re = 700 are shown in figure 10. The hot fluid only just reaches the region close to the lower boundary. The particle-laden case in comparison with the single-phase case does not transport the hot fluid as successfully downstream because of the peculiar cooling effect of the particles and the effective increase in heat capacity. The slight kink in the temperature contours between $x = 12$ and $x = 20$ is caused by the presence of the particles increasing the heat capacity; thereby, lowering the fluid's temperature.

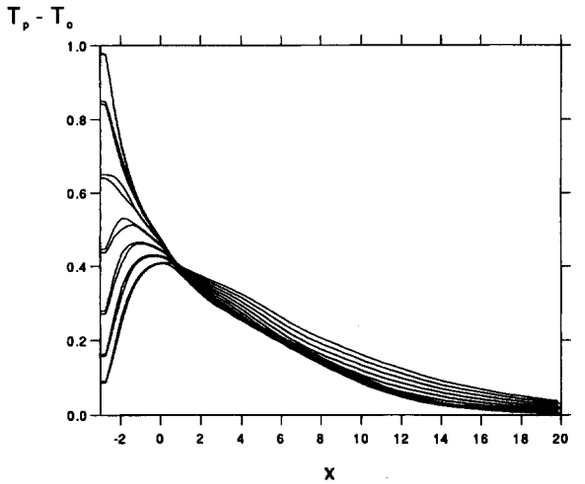

Figure 9 Temperature histories of various particles with respect to the x-coordinate, case (8)

Conclusion

Introduction of a stream of low-Stokes number particles tends to generate stronger lower and upper recirculation regions. This is because the particles increase the inertia of the free-stream of the flow by overshooting the streamlines near the sudden expansion region. The upper separation position is mainly influenced by the lower reattachment position. The buoyancy-effect in the present configuration tends to cause a slight upward force near the sudden expansion, which suppresses the upper recirculation and causes longer lower reattachment lengths.

The thermophoresis effect was most significant in the x-direction caused by the gradually cooling fluid. The particles gain a slight increase in momentum, which further increases the inertia of the free stream and causes stronger recirculation regions.

The particles' higher heat capacity effectively increases the heat capacity of the fluid, which in this study, caused the fluid to reduce in temperature near the stream of the particles. The

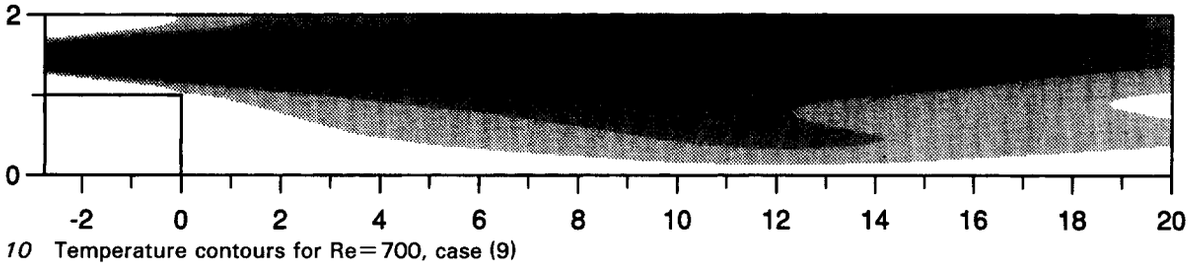

Figure 10 Temperature contours for Re=700, case (9)

effect was primarily caused by the fluid temperature rapidly diffusing outwards near the inlet.

Acknowledgment

The author thanks Ms A. Field for her comments on the original manuscript. I also thank Dr. I. M. Hall for valuable discussions on the subject.

Appendix

The equation of motion for a particle can be assumed to be of the form:

$$\frac{\partial u_p}{\partial t} = \frac{u_f - u_p}{\tau_p} \tag{A1}$$

Where u_p is the particle's velocity, u_f is the displaced fluid velocity, and τ_p is the particle relaxation time, which is $\rho_p d_p^2/18\mu$. The above equation is also in the same form as the equation that governs the temperature of the particle. The integration is achieved by assuming that the u_f or T_f values vary quadratically over the present and last time-step. It can, therefore, be expressed in the following form for u_f:

$$u_f(t) = u_f^n + At + Bt^2$$

$$A = \frac{u_f^{n+1^*}(\Delta t^{n-1})^2 + u_f^n[(\Delta t^n)^2 - (\Delta t^{n-1})^2] - u_f^{n-1}(\Delta t^n)^2}{\Delta t^{n-1}\,\Delta t^n(\Delta t^{n-1} + \Delta t^n)}$$

$$B = \frac{u_f^{n-1}\,\Delta t^n + u_f^{n+1^*}\,\Delta t^{n-1} - u_f^n(\Delta t^n + \Delta t^{n-1})}{\Delta t^{n-1}\,\Delta t^n(\Delta t^{n-1} + \Delta t^n)} \tag{A2}$$

Similar expressions can be found for the temperature integration. The superscript n refers to the current time level. The $n+1$ time level is, therefore, unknown, and a predicted value is expressed as $u_f^{n+1^*}$. The predicted value is found initially assuming $A = 0$ and $B = 0$; this is simply the application of the standard Lagrangian tracking scheme. The values of A and B are then found using the predicted value $u_f^{n+1^*}$, the values A and B are then updated, and the final solution is found. This means the procedure is repeated twice; e.g., there are two prediction levels and one correction level. The temperature integration requires only one level, because after the velocity and position have been integrated, the current position and the "future" position are known.

The general solution of the particle's velocity and position are expressed as:

$$U_p^{n+1} = U_p^n \exp\frac{-\Delta t}{\tau_p} + U_f^n\left(1 - \exp\frac{-\Delta t}{\tau_p}\right) + A\left[\Delta t - \tau_p\left(1 - \exp\frac{-\Delta t}{\tau_p}\right)\right] + B\left[\Delta t^2 - 2\tau_p\,\Delta t + 2\tau_p^2\left(1 - \exp\frac{-\Delta t}{\tau_p}\right)\right] \tag{A3}$$

and

$$x_p^{n+1} = x_p^n + \tau_p(U_f^n - U_p^n)\left(1 - \exp\frac{-\Delta t}{\tau_p}\right) + A\left[\frac{\Delta t^2}{2} - \tau_p\,\Delta t + \tau_p^2\left(1 - \exp\frac{\Delta t}{\tau_p}\right)\right] + B\left[\frac{\Delta t^3}{3} - \tau_p\,\Delta t^2 + 2\tau_p^2\,\Delta t - 2\tau_p^3\left(1 - \exp\frac{-\Delta t}{\tau_p}\right)\right] \tag{A4}$$

The temperature solution is in the same form as the velocity general solution.

References

Abbas, A. S., Koussa, S. S. and Lockwood, F. C. 1980. The prediction of the particle-laden flows. Imperial College Rep. FS/80/1, London, UK

Abu-Mulaweh, H. I., Armaly, B. F. and Chen, T. S. 1993. Measurements of laminar mixed-convection in boundary-layer flow over horizontal and inclined backward-facing steps. *Int. J. Heat Mass Transfer*, **36**, 1883–1895

Anderson, D. A., Tannehill, J. C. and Pletcher, R. H. 1984. *Computational Fluid Mechanics and Heat Transfer*. Hemisphere, Bristol, PA

Armaly, B. F., Durst, F., Pereira, J. C. F. and Schönung, B. 1983. Experimental and theoretical investigation of backward-facing step flow. *J. Fluid Mech.*, **127**, 473–496

Aung, W. 1983. An experimental study of laminar heat transfer downstream of backsteps. *J. Heat Transfer*, **105**, 823–829

Barton, I. E. 1994. Laminar flow past an enclosed and open backward-facing step. *Phys. Fluids*, **6**, 4054–4056

Barton, I. E. 1995. Computation of incompressible particulate flows. Ph.D. thesis, Department of Engineering, University of Manchester, Manchester, UK

Barton, I. E. 1996a. Computation of dilute particulate laminar flow over a backward facing step. *Int. J. Numer. Meth. Fluids*, **22**, 211–221

Barton, I. E. 1996b. Exponential Lagrangian tracking schemes applied to Stokes law. *J. Fluids Eng.*, **118**, 85–89

Blosch, E., Shyy, W. and Smith, R. 1993. The role of mass conservation in pressure-based algorithms. *Numer. Heat Transfer*, **B 24**, 415–429

Boyd, R. K. and Kent, J. H. 1986. Three-dimensional furnace computer modelling. *Proc. 21st Symposium (Int.) on Combustion*, The Combustion Institute, 265–274

Boysan, F., Ayres, W. H. and Swithenbank, J. 1982. A fundamental mathematical modelling approach to cyclone design. *Trans. Inst. Chem. Eng.*, **60**, 222–230

Caruso, S. C., Ferziger, J. H. and Oliger, J. 1986. Adaptive grid techniques for elliptic fluid flow problems. *Proc. AIAA 24th Aerospace Sciences Meeting* (Reno, NV), AIAA, New York, Paper 86-0498

Celik, I. 1988. Isothermal prediction of particle and gas flow in a coal-fired reactor. *Particulate Sci. Tech.*, **6**, 53–68

Chao, Y. C. and Liu, S. S. 1991. Streamline adaptive grid method for complex flow computation. *Numer. Heat Transfer*, **B 20**, 145–168

Crowe, C. T., Sharma, M. P. and Shock, D. E. 1977. The particle-source-in cell (PSI-cell) model for gas droplet flows. *J. Fluids Eng.*, 325–332

Durst, F., Milojevic, D. and Schönung, B. 1984. Eulerian and Lagrangian predictions of particulate two-phase flows: A numerical study. *Appl. Math. Modelling*, **8**, 101–115

Durst, F. and Pereira, J. C. F. 1988. Time-dependent laminar backward-facing step flow in a two-dimensional duct. *J. Fluids Eng.*, **110**, 289–296

Gartling, D. K. 1990. A test problem for outflow boundary conditions —Flow over a backward-facing step. *Int. J. Numer. Meth. Fluids*, **11**, 953–967

Gosman, A. D. and Ioannides, E. 1983. Aspects of computer simulation of liquid-fueled combustors. *J. Energy*, 7, 482–490

Gresho, P. M. 1991. Letter to the editor. *Numer. Heat Transfer*, **A 20**, 123

Guj, G. and Stella, F. 1988. Numerical solutions of high-Re recirculating flows in vorticity–velocity form. *Int. J. Numer. Meth. Fluids*, **8**, 405–416

Hall, E. J. and Pletcher, R. H. 1985. Application of a viscous–inviscid interaction procedure to predict separated flows with heat transfer. *J. Heat Transfer*, **107**, 557–563

Harlow, F. H. and Welch, J. E. 1965. Numerical calculations of time-dependent viscous incompresible flow of fluid with free surface. *Phys. Fluids*, **8**, 2182–2189

Hétu, J.-F. and Pelletier, D. H. 1992. Adaptative remeshing for viscous incompressible flows. *AIAA J.*, **30**, 1986–1992

Kim, J. and Moin, P. 1985. Application of a fractional-step method to incompressible Navier–Stokes equations. *J. Comp. Phys.*, **59**, 308–323

Kobayashi, M. H., Pereira, J. C. F. and Sousa, J. M. M. 1993. Comparison of several open boundary numerical treatments for laminar recirculating flows. *Int. J. Numer. Meth. Fluids*, **16**, 403–419

Kondoh, T., Nagano, Y. and Tsuji, T. 1993. Computational study of laminar heat transfer downstream of a backward-facing step. *Int. J. Heat Mass Transfer*, **36**, 577–591

Lee, D. and Tsuei, Y. M. 1993. A hybrid adaptive gridding procedure for recirculating fluid flow problems. *J. Comp. Phys.*, **108**, 122–141

Leone, J. M., Jr. 1990. Open boundary condition symposium benchmark solution: Stratified flow over a backward-facing step. *Int. J. Meth. Fluids*, **11**, 969–984

Leschziner, M. A. 1980. Practical evaluation of three finite-difference schemes for the computation of steady-state recirculating flows. *Comp. Meth. Appl. Mech. Eng.*, **23**, 293–312

Lin, J. T., Armaly, B. F. and Chen, T. S. 1990. Mixed convection in buoyancy-assisting vertical backward-facing step flows. *Int. J. Heat Mass Transfer*, **33**, 2121–2132

Lin, J. T., Armaly, B. F. and Chen, T. S. 1991. Mixed-convection heat transfer in inclined backward-facing step flows. *Int. J. Heat Mass Transfer*, **34**, 1568–1571

Lockwood, F. C., Salooja, A. P. and Syed, S. A. 1980. A prediction method for coal-fired furnaces. *Combustion & Flame*, **38**, 1–15

Migdal, D. and Agosta, V. D. 1967. A source flow model for continuous gas-particle flow. *J. Fluid Eng.*, **34**, 860–865

Morgan, K., Periaux, J. and Thomasset, F. 1984. Analysis of laminar flow over a backward-facing step. In *Notes on Numerical Fluid Mechanics*, Vol. 9, Vieweg

Mostafa, A. A. 1991. Modelling of densely loaded two-phase flows. *Numer. Heat Transfer*, **A 20**, 317–328

Orlandi, P. 1987. Vorticity–velocity formulation for high Re flows. *Computers & Fluids*, **15**, 137–149

Patankar, S. V. 1980. *Numerical Heat Transfer and Fluid Flow*. Hemisphere, Bristol, PA, 1090–1093

Patankar, S. V., Karki, K. C. and Mongia, H. C. 1987. Development and evaluation of improved numerical schemes for recirculating flows. *Proc. AIAA 25th Aerospace Sciences Meeting* (Reno, NV), AIAA, New York, Paper 87-0061

Patankar S. V. and Spalding, D. B. 1972. A calculation procedure for heat, mass, and momentum transfer in three-dimensional parabolic flows. *Int. J. Heat Mass Transfer*, **15**, 1787–1806

Ruck, B. and Makiola, B. 1988. Particle dispersion in a single-sided backward-facing step flow. *Int. J. Multiphase Flow*, **14**, 787–800

Sani, R. L. and Gresho, P. M. 1994. Résumé and remarks on the open boundary condition minisymposium. *Int. J. Numer. Meth. Fluids*, **18**, 983–1008

Shyy, W. 1985. A study of finite-difference approximations to steady-state, convection-dominated flow problems. *J. Comp. Phys.*, **57**, 415–438

Sohn, J. L. 1988. Evaluation of FIDAP on some classical laminar and turbulent benchmarks. *Int. J. Numer. Meth. Fluids*, **8**, 1469–1490

Soo, S. L. 1982. *Multiphase Fluid Dynamics*. Science Press, Gower Technical

Soong, C. Y. and Hsueh, W. C. 1993. Mixed convection in a suddenly expanded channel with effects of cold fluid injection. *Int. J. Heat Mass Transfer*, **36**, 1477–1484

Sparrow, E. M. and Chuck, W. 1987. PC solutions for heat transfer and fluid flow downstream of an abrupt, asymmetric enlargement in a channel. *Numer. Heat Transfer*, **12**, 19–40

Thangam, S. and Knight, D. D. 1989. Effect of step height on the separated flow past a backward-facing step. *Phys. Fluids*, **1**, 604–606

Thangam, S. and Knight, D. D. 1990. A computational scheme in generalized coordinates for viscous incompressible flows. *Computers & Fluids*, **18**, 317–327

Vogel, J. C. and Eaton, J. K. 1985. Combined heat transfer and fluid dynamic measurements downstream of a backward-facing step. *J. Heat Transfer*, **107**, 922–929

Vradis, G. C. and VanNostrand, L. 1992. Laminar coupled flow downstream of an asymmetric sudden expansion. *J. Thermophys. Heat Transfer*, **6**, 288–295

Walker, K. L., Geyling, F. T. and Nagel, S. R. 1980. Thermophoretic deposition of small particles in the modified chemical vapor deposition (MCVD) process. *J. Am. Ceram. Soc.*, **63**, 552–558